On the invariance of flame-motion-induced variations of the generalized disturbance energy

Jean-Michel Klein, Albane Gandilhon-Gounelle, Axel Vincent-Randonnier, Aurelien Genot, Arnaud Mura

On the invariance of flame-motion-induced variations of the generalized disturbance energy

Jean-Michel Klein, Albane Gandilhon-Gounelle, Axel Vincent-Randonnier, Aurelien Genot[a], Arnaud Mura [b,*]

[a] *DMPE, ONERA, Université Paris Saclay F-91123 Palaiseau - France,*
[b] *PPRIME UPR3346 CNRS, ENSMA and University of Poitiers, 1 Avenue Clément Ader, 86961 Futuroscope Chasseneuil, France,*

Abstract

The response of a one-dimensional laminar premixed flame to an inlet velocity forcing is investigated within the disturbance energy budget (DEB) framework. It is evidenced that the flame behaviour can be characterized through two dimensionless numbers. The first is a Strouhal number St, which is related to the flame motion and compares the flame front flapping length scale to the laminar premixed flame thickness δ_L^0. The second is the normalized velocity forcing level η, i.e., the ratio between the amplitude of the inlet velocity variation and the laminar flame speed. Among the various disturbance energy sources, three terms, which do involve temperature (entropy) fluctuations, have significant growth-rates. These are: (i) the thermoacoustic source, (ii) an entropic term related to the coupling between entropy and temperature gradient variations, and finally (iii) a sink term relevant to thermal diffusion effects. For moderate forcing levels, the sole knowledge of these three terms together with St are sufficient to describe the flame dynamics. However, for larger forcing levels, the aforementioned contributions are no longer predominant over the transient variations of the disturbance energy that are induced by velocity fluctuations. Indeed, although the growth-rates of the corresponding source terms remain marginal — regardless of forcing amplitude and frequency — they must be taken into account so as to predict the evolution of the system, and the second non-dimensional number η becomes necessary to proceed with its precise characterization.

Keywords: thermoacoustics, flame motion, disturbance energy budget

*Corresponding author.
Email address: arnaud.mura@ensma.fr (Arnaud Mura)

Nomenclature

Latin letters

a	:	speed of sound $[\mathrm{m}\cdot\mathrm{s}^{-1}]$
c	:	temperature progress variable
D_j	:	disturbance energy source $[\mathrm{J}\cdot\mathrm{s}^{-1}\cdot\mathrm{m}^{-3}]$
$\mathcal{D}_j$	:	volume integrated source $[\mathrm{J}\cdot\mathrm{s}^{-1}]$
E_a	:	acoustic energy $[\mathrm{J}\cdot\mathrm{m}^{-3}]$
E_d	:	disturbance energy $[\mathrm{J}\cdot\mathrm{m}^{-3}]$
$\mathcal{E}_d$	:	volume-integrated disturbance energy [J]
e_t	:	total specific energy $[\mathrm{J}\cdot\mathrm{kg}^{-1}]$
f	:	frequency [Hz]
g_k	:	Gibbs free energy of chemical species k $[\mathrm{J}\cdot\mathrm{kg}^{-1}]$
G_χ	:	gain relevant to the variable χ
h_k	:	enthalpy of chemical species k $[\mathrm{J}\cdot\mathrm{kg}^{-1}]$
H	:	total enthalpy $[\mathrm{J}\cdot\mathrm{kg}^{-1}]$
L	:	computational domain length [m]
Le_k	:	Lewis number of chemical species k
$\boldsymbol{m}$	:	mass flux $[\mathrm{kg}\cdot\mathrm{m}^{-2}\cdot\mathrm{s}^{-1}]$
N	:	number of chemical species
p	:	pressure [Pa]
Pr	:	Prandtl number
$\dot{q}$	:	heat release rate HRR $[\mathrm{J}\cdot\mathrm{m}^{-3}\cdot\mathrm{s}^{-1}]$
$\dot{Q}$	:	volume-averagedd HRR $[\mathrm{J}\cdot\mathrm{m}^{-3}\cdot\mathrm{s}^{-1}]$
S_L^0	:	laminar premixed flame speed $[\mathrm{m}\cdot\mathrm{s}^{-1}]$
s	:	entropy $[\mathrm{J}\cdot\mathrm{kg}^{-1}\cdot\mathrm{K}^{-1}]$
S_R	:	Rayleigh index $[\mathrm{J}\cdot\mathrm{s}^{-1}]$
St	:	Strouhal number $\mathrm{St} = 2\pi f\delta_L^0/(\eta S_L^0)$ $[-]$
St_F	:	Strouhal number $\mathrm{St}_F = f\delta_L^0/S_L^0$ $[-]$
t	:	time [s]
T	:	temperature [K]
$\mathcal{T}$	:	arbitrary time interval [s]
$\boldsymbol{v}$	:	velocity $[\mathrm{m}\cdot\mathrm{s}^{-1}]$

v_F : flame front velocity [$\mathrm{m \cdot s^{-1}}$]
$\mathcal{V}$: arbitrary volume [$\mathrm{m^3}$]
v_p : velocity perturbation [$\mathrm{m \cdot s^{-1}}$]
$\boldsymbol{V_k}$: diffusion velocity of species k [$\mathrm{m \cdot s^{-1}}$]
$\boldsymbol{W}$: disturbance energy flux vector [$\mathrm{J \cdot s^{-1} \cdot m^{-2}}$]
$\mathcal{W}$: disturbance energy total boundary flux [$\mathrm{J \cdot s^{-1}}$]
x : axial coordinate [m]
x_F : flame position [m]
Y_k : mass fraction of chemical species k

Subscripts and superscripts

0 : related to the baseline value (as a subscript) or to laminar flame (as a superscript)
1 : related to the fluctuation (as a subscript)
$*$: related to non-dimensional quantities (superscript) or to a DEB source term (subscript)
b : related to fully burned products of combustion
k : related to chemical species k
p : related to perturbation applied at the inlet boundary condition
u : related to unburned fresh reactants

Greek letters

α : growth-rate [$\mathrm{s^{-1}}$]
γ : ratio of heat capacities
δ_L^0 : thermal flame thickness [m]
η : velocity forcing level
λ : heat conductivity [$\mathrm{J \cdot s^{-1} \cdot \ m^{-1} \cdot K^{-1}}$]
ρ : density [$\mathrm{kg \cdot m^{-3}}$]
$\boldsymbol{\tau}$: viscous stress tensor [Pa]
χ : generic variable
$\dot{\omega}_k$: reaction rate of species k [$\mathrm{kg \cdot m^{-3} \cdot s^{-1}}$]
$\boldsymbol{\Omega}$: vorticity [$\mathrm{s^{-1}}$]

Acronyms

AP	:	additional perturbation
DEB	:	disturbance energy budget
ER	:	equivalence ratio
FD	:	flame dynamics
FIR	:	flame intensity response
FM	:	flame motion
FT	:	flame thickening
HRR	:	heat-release rate
RHS	:	right-hand side
RMS	:	root mean square
VP	:	velocity perturbation

Operators

$\overline{q}$	:	time-averaged value of quantity q
q_0	:	reference or baseline value of quantity q
q_1	:	fluctuations of quantity q
$\boldsymbol{\nabla}$	:	vectorial operator (gradient)

1. Introduction and general context

Combustors are known to be prone to self-sustained instabilities [1] which may strongly damage them as a result of mechanical and thermal stresses induced by large variations of pressure and temperature. The Rayleigh criterion[1] offers a long-standing tool to predict such combustion instabilities [2, 3, 4, 5, 6]. In this respect, it can be shown that the corresponding Rayleigh term is indeed one of the contributions that appear in the conservation equation for the classical acoustic energy $E_a = \rho_0 (\boldsymbol{v}_1 \cdot \boldsymbol{v}_1)/2 + p_1^2/(2\rho_0 a_0^2)$, a budget that can be derived by making use of linearization procedures [7, 8]. In the expression of E_a, the quantities ρ, $\boldsymbol{v}$, p, and a denote the density, velocity vector, pressure, and speed of sound. Moreover, it does not seem useless to recall that, in this expression, the subscript 1 refers to "small-amplitude fluctuations" superimposed on the "baseline" flow (subscript 0). Various forms of such a conservation equation have been early proposed in the literature, see for instance [9], with some of them including inhomogeneities, mean flow effects, and/or heat addition [10, 11]. In this respect, the work of Morfey [10] does provide a comprehensive survey of acoustic energy conservation in non-uniform flows including comparisons with classical acoustics results (i.e., small-amplitude perturbations in a fluid otherwise at rest). The consideration of the combustion-induced heat release rate (HRR) in such an acoustic budget leads to the Rayleigh source term, i.e., $(\gamma - 1)\dot{q}_1 p_1/(\gamma p_0)$ with γ the ratio of heat capacities and $\dot{q}_1$ the HRR fluctuation. This contribution – which is directly related to the coupling between heat release rate and pressure variations – does appear as a source term in this budget.

Once integrated over time $\mathcal{T}$ in the flow domain $\mathcal{V}$, it leads to the Rayleigh

[1] It is noteworthy that a mathematical formulation of this criterion was subsequently proposed by Putnam and Dennis [2], see also reference [3] for its more detailed presentation.

index [12]

$$\mathrm{S_R} = \frac{(\gamma-1)}{\gamma\, p_0}\,\frac{1}{\mathcal{T}}\int_{\mathcal{V}}\int_{\mathcal{T}} \dot{q}_1\; p_1\; dt\; dv \tag{1}$$

from which the Rayleigh criterion is deduced: the combustor may become unstable if the HRR variations are in phase with the pressure variations [2, 4, 5]. Put in other words, if heat is added during the compression phase of the acoustic cycle and removed during the expansion phase, the level of pressure variations gets amplified by the heat addition process.

However, as emphasized by Nicoud and Poinsot [8], the above condition may be thought as a necessary – rather than a sufficient – condition for instability to occur. As a matter of fact, following the early proposal of Chu [13] – and instead of considering the classical acoustic energy conservation – the possible relevance of a disturbance energy budget (DEB) that includes, among others, the contribution of entropy fluctuations has been also discussed in the literature [14, 15, 16, 17, 18]. Thus, the disturbance energy E_d can take into account the non-negligible entropy fluctuations that can be induced by the flame front motion [19, 20], which, in turn, leads to consider additional entropy sources in its conservation equation. The considered disturbance energy is thereby the consequence of the choice of relevant primitive variables – the most common being the fluctuations of pressure p_1, velocity $\boldsymbol{v}_1$, and entropy s_1 – and some previous studies have been focused on how it could be properly defined and evaluated consistently with the underlying physics, see for instance [21, 22].

Another interesting direction was recently followed by Chen et al. [19]. They proposed a linearized framework to analyze a moving premixed flame front – with the flame considered as a discontinuity (i.e., compact acoustic source[2]) – and stud-

[2] Acoustic and entropy wavelengths are assumed to be much larger than the flame thickness.

ied its response to various kinds of perturbations. This analysis provides new insights into the consequences of flame front movement on acoustic scattering and entropy generation. Acoustic perturbations at a flame indeed lead to entropy variations that are associated to temperature inhomogeneities. They are convected by the flow and often referred to as entropy waves or entropy spots. Such inhomogeneities may experience acceleration which in turn give rise to acoustic waves [23, 24]. The impact of flame dynamics has been also revisited on the basis of an energetic approach by Méry [25, 26]. Consistently with the compact source approximation, the flame is considered infinitely thin and the HRR expressed as $\dot{q}(\boldsymbol{x},t) = \dot{Q}(t)\,\delta(\boldsymbol{x}^* - \boldsymbol{x}_F^*(t))$ with $\dot{Q}(t)$ its value integrated across the flame and $\boldsymbol{x}_F^*(t)$ the properly-normalized flame position in the laboratory frame of reference. Making use of this expression, the integral contribution of the Rayleigh term, i.e., Eq.(1), becomes

$$\begin{aligned} \mathrm{S_R} &= \frac{(\gamma-1)}{\gamma\, p_0}\,\frac{1}{\mathcal{T}}\int_{\mathcal{V}}\int_{\mathcal{T}} \dot{Q}(t)\,\delta(\boldsymbol{x}^* - \boldsymbol{x}_F^*(t))\; p_1(\boldsymbol{x}^*,t)\; dt\; dv \\ &= \frac{(\gamma-1)}{\gamma\, p_0}\,\frac{1}{\mathcal{T}}\int_{\mathcal{T}} \dot{Q}(t)\; p_1(\boldsymbol{x}_F^*(t),t)\; dt \end{aligned} \tag{2}$$

By expressing $\dot{Q}(t)$ as the sum of $\dot{Q}_0$ – the global or baseline HRR – and $\dot{Q}_1$ – the unsteady HRR in the flame frame of reference – it can be subsequently decomposed into two distinct parts

$$\mathrm{S_R} = \frac{(\gamma-1)}{\gamma\, p_0}\,\frac{1}{\mathcal{T}}\int_{\mathcal{T}} \dot{Q}_1(t)\; p_1(\boldsymbol{x}_F^*(t),t)\; dt + \frac{(\gamma-1)}{\gamma\, p_0}\,\frac{\dot{Q}_0}{\mathcal{T}}\int_{\mathcal{T}} p_1(\boldsymbol{x}_F^*(t),t)\; dt \tag{3}$$

which are related to "flame response contribution" (first term in the right-hand side (RHS) of Eq.(3)) and to "flame motion contribution" (second term in the RHS of Eq.(3)), respectively. The former represents the flame response to upstream

velocity perturbations, a contribution that has been represented within the $n-\tau$ modelling framework [27] in reference [26]. This contribution is relevant to the temporal variation of the global HRR, i.e., $d\dot{Q}/dt$. The second term in the RHS of Eq.(3) is referred to as the "flame motion contribution" and it is related to the fluctuations of the flame position $\boldsymbol{x}_F(t)$: it can be non-zero even if $d\dot{Q}/dt = 0$.

From a general point of view, the flame response contribution, i.e., the temporal variations of the integral $\dot{Q}(t) = (1/\mathcal{V})\int_{\mathcal{V}} \dot{q}(\boldsymbol{x},t)dv$ can result from either (i) variations of the HRR across the local flame front, hereafter referred to as the "flame intensity response" (FIR) or (ii) variations of the available amount of flame surface, e.g., production induced by wrinkling processes or destruction through kinematic restoration [28, 29, 30]. In this respect, the flame transfer function is one of the frameworks that allows to characterize, and model, the flame response to velocity perturbations [26, 31, 32]. Since equivalence ratio has a direct influence on the level of heat release, its fluctuations obviously lead to temporal variations of $\dot{Q}(t)$ and, therefore, the flame response to equivalence ratio (ER) fluctuations has been early documented in the literature [33, 34, 35]. At this level, it is noteworthy that the flame front acts as a low-pass filter and, as a consequence, some of the previous effects may be damped at high frequencies [36, 37]. The corresponding high-frequency response can be characterized by using a flame Strouhal number $\mathrm{St}_F = f\delta_L^0/S_L^0$ with f, S_L^0, and δ_L^0 the perturbation frequency, laminar premixed flame speed and thickness [37]. Finally, albeit not detailed herein, other types of perturbation associated to entropy [38] or pressure fluctuations [39, 40] may alter the flame response and may even become dominant over the possible influence of velocity perturbations in high-frequency regimes characterized by values of St_F larger than unity.

If one excepts situations relevant to the impact of transverse acoustic waves [41, 25, 42] or high power density systems [26], it must be recognized that the flame

motion contribution – i.e., the second term present in the RHS of Eq.(3) – has been often overlooked compared to the flame response contribution. However, as emphasized above, there is a consensus in the literature on the need to account entropy fluctuations when dealing with combustion thermoacoustics [8, 21, 22]. Therefore, the Rayleigh index given by Eqs.(1)-(3), which is the integral outcome of the Rayleigh source term involved in an acoustic energy budget that does not account for entropy variations, might not be sufficient [8]. For instance, in the case of combustion flashback or blow-off [43, 44, 45] the flame location is strongly varying and the corresponding motion is associated to significant levels of entropy fluctuations, which are not explicitly taken into account within the Rayleigh index framework. The definition of some more sophisticated criteria including the effects of entropy fluctuations [13] and non-linearities [14, 18] offers thereby a promising way to analyze combustion stability in more relevant (and also more complex) flows at the industrial scale.

The present work is devoted to a new analysis of disturbance energy production resulting from the motion of a laminar premixed flame which is subject to inlet perturbations. There exist several ways to trigger the unsteady motion of a laminar premixed flame. One may consider, for instance, perturbations in the inlet ER. However, it must be acknowledged that the influence of inlet ER variations on laminar premixed flames has already received considerable attention in previous theoretical [35, 46], experimental [33, 34, 47, 48, 49], and computational studies [50, 51, 52]. Moreover, as stated above, ER fluctuations would also trigger non-negligible effects relevant to the flame intensity response (FIR) and this would require to discriminate them from the flame motion contribution on which the present study is focused. Therefore, the possible effects of inlet ER fluctuations are not considered and present analysis is concerned only with the consequence of inlet velocity perturbations on fully premixed conditions. This work makes

use of the energy corollary introduced by Myers [14] that has been subsequently extended to the transport of the disturbance energy in multicomponent reactive flows [15, 16, 18]. The corresponding DEB framework offers the opportunity to circumvent possible limitations of the classical acoustic energy budget and this disturbance energy corollary includes the transport of multiple chemical species as well as chemical non-equilibrium and heat release contributions [15, 18]. Moreover, in contrast with the classical acoustic energy E_a, the disturbance energy E_d and its conservation equation are obtained without any resort to linearization procedures and large-amplitude disturbances can be taken into account. The source terms that appear in this disturbance energy budget are scrutinized through a parametric computational study performed on one-dimensional laminar premixed flames with imposed inlet velocity variations.

The manuscript is organized as follows: the computational setup and reference laminar premixed flame are first presented in section 2. Section 3 describes the inlet velocity perturbation and the post-processing methodology that is based on the disturbance energy budget (DEB). Following the previous work of Méry [26] some definitions are then introduced in an attempt to characterize and discriminate the various DEB contributions (section 4). Then, in the continuity of previous studies devoted to the definition of time and length scales relevant to flame-acoustic interactions [37], two dimensionless numbers are introduced. The first is a Strouhal number based on the laminar premixed flame transit time, inlet fluctuation frequency, and forcing amplitude. The second is the normalized velocity forcing level, i.e., the ratio between the inlet velocity variation amplitude and the laminar flame speed. The relevance of the corresponding numbers in the DEB scaling is highlighted in section 5. Finally, some conclusions and prospects for future work are gathered in section 6.

2. Numerical simulations

2.1. Computational setup

Numerical simulations are performed with the ONERA computational fluid dynamics (CFD) solver CEDRE [53, 54, 55, 56, 57].

The following set of one-dimensional compressible reactive Navier-Stokes equations is considered:

$$\frac{\partial}{\partial t}(\rho v) + \frac{\partial}{\partial x}(\rho v v) = -\frac{\partial p}{\partial x} + \frac{\partial \tau_{xx}}{\partial x} \tag{4}$$

$$\frac{\partial}{\partial t}(\rho e_t) + \frac{\partial}{\partial x}(\rho v e_t) = \frac{\partial}{\partial x}\left(\lambda \frac{\partial T}{\partial x} - \rho \sum_{k=1}^{k=N} h_k Y_k V_{k,x}\right) + \frac{\partial}{\partial x}(\tau_{xx} v) \tag{5}$$

$$\frac{\partial}{\partial t}(\rho Y_k) + \frac{\partial}{\partial x}(\rho v Y_k) = -\frac{\partial}{\partial x}(\rho Y_k V_{k,x}) + \dot{\omega}_k \tag{6}$$

where t denotes time, x the longitudinal coordinate and associated direction, ρ the density, v the velocity component along the x-direction, p the pressure, $\boldsymbol{\tau}$ the viscous stress tensor, λ the thermal diffusivity, and $e_t = e + vv/2$ the total specific energy. The quantities Y_k, V_k, $\dot{\omega}_k$, and h_k (with $k = 1, ..., N$) stand for the chemical species mass fractions, diffusion velocities, reaction rates, and enthalpies, respectively.

The computational setup is a one-dimensional domain of length $L = 15$ mm discretized with 5000 computational cells of size $\Delta x = 3$ μm, see Fig. 1. This ensures a satisfactory spatial resolution of the premixed flame front with approximately 150 computational points in its thickness. The temporal integration is performed with a second-order Runge-Kutta scheme [58] and spatial discretization makes use of a second-order multi-slope MUSCL scheme [59]. Finally, it is noteworthy that the unsteady solutions associated to inlet-velocity forcing, which are described in sections 3 and 4, have been obtained with a temporal discretization $\Delta t = 5 \times 10^{-8}$ s.

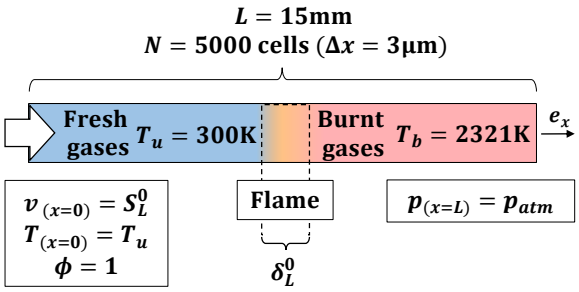

Figure 1: Sketch of the computational domain and reference premixed flame solution

A stoichiometric mixture of methane and air at temperature $T(x{=}0) = T_u =$ 300 K is injected on the left side of the computational domain. The outlet pressure is set to the atmospheric pressure ($p(x = L) = 101300$ Pa) using a non-reflective boundary condition [60, 61], thus ensuring that the external forcing indeed drives the flame dynamics (the reflection coefficient is less than 0.2). A steady-state solution is obtained provided that the inlet velocity is set equal to the laminar premixed flame speed $v(x{=}0) = S_L^0 = 0.395\,\text{m}\cdot\text{s}^{-1}$.

Chemical reaction is described with a single-step chemistry model, the relevance of which for studying premixed flames has been assessed elsewhere, see for instance [62, 63]. Molecular transport is modelled by assuming constant Lewis numbers together with a constant mixture Prandtl number, the values of which (see Tab. 1) have been set from a preliminary one-dimensional flame computation performed with the Cantera solver [64]. A Sutherland law and polynomial expressions are used to model the variations of the chemical species viscosity and heat capacity with temperature.

2.2. Steady flame computation

A reference one-dimensional stoichiometric premixed flame has first been computed with CEDRE and the obtained results have been compared to those issued

Table 1: Molecular transport properties

Prandtl number Pr	Lewis numbers Le_k				
	CH_4	O_2	N_2	CO_2	H_2O
0.71	0.97	1.11	1.02	1.34	0.77

from the computation of a steady one-dimensional stoichiometric premixed flame performed with the Cantera solver [64].

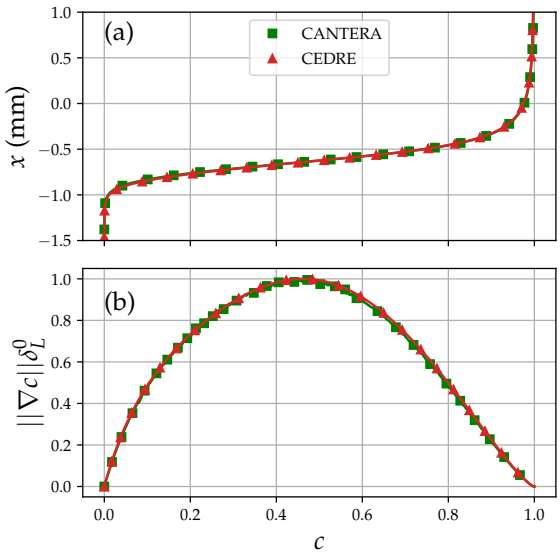

Figure 2: Steady flame computation: comparisons between CEDRE and Cantera solutions. Progress variable profile against the x-coordinate (top) and normalized progress variable gradient $\|\boldsymbol{\nabla} c\|\delta_L^0$ plotted versus the progress variable c (bottom)

Figure 2 displays the evolution of the progress variable $c = (T - T_u)/(T_b - T_u)$ together with the normalized progress variable gradient $\|\boldsymbol{\nabla} c\|\delta_L^0$. The results obtained with CEDRE and Cantera are quite consistent and only slight differences are observed for both the thermal flame thickness δ_L^0 and laminar flame propagation velocity S_L^0, see Tab. 2.

Table 2: Comparison between laminar premixed flame characteristics issued from CEDRE and Cantera computations

	Cantera	CEDRE	Difference
δ_L^0	420 μm	444 μm	5.7%
S_L^0	0.393 m $\cdot$ s^{-1}	0.395 m $\cdot$ s^{-1}	0.3%

3. Disturbance energy budget (DEB)

The one-dimensional laminar premixed flame presented in the previous section is now subject to a pulsed inlet velocity:

$$v(x=0,t) = S_L^0(1+\eta\cos(2\pi f t)) = S_L^0 + v_p(x=0,t) \tag{7}$$

with $v_p(x=0,t) = \eta S_L^0 \cos(2\pi f t)$ the inlet velocity perturbation. A reference simulation is first conducted with $f = 100$ Hz the disturbance frequency, and $\eta = 0.05$ the dimensionless amplitude of the velocity fluctuation normalized with respect to the laminar flame speed. The flame response to these velocity perturbations is analyzed within the generalized disturbance energy framework.

The transport equation introduced by Giauque et al. [16, 15] for the disturbance energy E_d writes:

$$\frac{\partial E_d}{\partial t} + \boldsymbol{\nabla}\cdot\boldsymbol{W} = D \tag{8}$$

where $\boldsymbol{W} = \boldsymbol{m_1} H_1 - T_0 \boldsymbol{m_1} s_1 + \boldsymbol{m_0} T_1 s_1$ is the disturbance energy flux vector, which can be recast so as to put into evidence the acoustic and entropy perturbations fluxes [65]. The quantity D stands for the sum of the various source terms that are responsible for disturbance energy production [18]. The detailed expressions of each contribution to this source term are reported in Tab. 3. In these expressions, the quantities H, s, $\boldsymbol{m} = \rho\boldsymbol{v}$, $\boldsymbol{v}$, $\boldsymbol{\Omega}$, and $\dot{q}$ are the total enthalpy, entropy, mass flux,

velocity vector, vorticity vector, and combustion-induced heat release rate (HRR). Finally, g_k denotes the Gibbs free energy of chemical species k. The subscript 1 stands for the fluctuation of the corresponding quantity with respect to its baseline value (subscript 0), i.e., the steady flame of section 2.2 in the present study.

Table 3: Expressions of the various terms present in the disturbance energy budget (DEB) and global values deduced from the post-processing of the reference simulation

Term	Expression	Growth-rate
$\partial E_d/\partial t$	$\partial/\partial t(\rho(H_1 - T_0 s_1) - \boldsymbol{m_0}\cdot\boldsymbol{v}_1$ $-p_1 - \rho\sum_k g_{k0} Y_{k1})$	$+1.63$ s^{-1}
$\boldsymbol{\nabla}\cdot\boldsymbol{W_1}$	$\boldsymbol{\nabla}\cdot(\boldsymbol{m}_1 H_1 - T_0 \boldsymbol{m}_1 s_1)$	$+0.01$ s^{-1}
$\boldsymbol{\nabla}\cdot\boldsymbol{W_2}$	$\boldsymbol{\nabla}\cdot(\boldsymbol{m_0} T_1 s_1)$	≈ 0 s^{-1}
D_{s_1}	$\boldsymbol{m_0}\cdot\boldsymbol{\nabla} T_1 s_1$	$\mathbf{+3729}$ **s^{-1}**
D_{s_2}	$-\boldsymbol{\nabla} T_0\cdot\boldsymbol{m}_1 s_1$	$+0.12$ s^{-1}
D_Q^{comb}	$T_1\,(\dot{q}/T)_1$	$\mathbf{+4023}$ **s^{-1}**
D_Q^{cond}	$T_1(\boldsymbol{\nabla}\cdot(\lambda\boldsymbol{\nabla}T)/T)_1$	$\mathbf{-7251}$ **s^{-1}**
D_Q^{sp}	$-\sum_k T_1\,(\boldsymbol{\nabla}\cdot(\rho h_k Y_k \boldsymbol{V_k})/T)_1$	-6.88 s^{-1}
D_{Q^*}	$\sum_k T_1\,(g_k\boldsymbol{\nabla}\cdot(\rho\boldsymbol{V_k}Y_k) - g_k\dot{\omega}_k/T)_1$	-368 s^{-1}
$D_{\boldsymbol{\Omega}}$	$-\boldsymbol{m_1}\cdot(\boldsymbol{\Omega}\wedge\boldsymbol{v})_1$	≈ 0 s^{-1}
$D_{\boldsymbol{\Psi}}$	$\boldsymbol{m}_1\cdot\left(\rho^{-1}\boldsymbol{\nabla}\cdot\boldsymbol{\tau}\right)_1$	≈ 0 s^{-1}
D_{Y_1}	$\sum_k g_{k0}\,(\boldsymbol{m_1}\cdot\boldsymbol{\nabla}Y_{k1} + Y_{k1}\boldsymbol{\nabla}\cdot\boldsymbol{m_1})$	$+0.03$ s^{-1}
D_{Y_2}	$\sum_k g_{k1}\,(\dot{\omega}_{k1} - \boldsymbol{\nabla}\cdot(\rho\boldsymbol{V_k}Y_k)_1 - \boldsymbol{m_0}\cdot\boldsymbol{\nabla}Y_{k1})$	-0.01 s^{-1}

The various source terms are as follows: $D_s = D_{s_1} + D_{s_2}$ refers to sources related to indirect entropy fluctuations caused by the flame motion, D_Q^{comb} is the thermoacoustic source term related to unsteady HRR oscillations, D_Q^{cond} is relevant to thermal diffusion and D_Q^{sp} to chemical species diffusion, D_{Q^*} is related to the contribution of chemical species to thermoacoustic coupling. The quantity $D_{\boldsymbol{\Omega}}$ is related to vorticity, $D_{\boldsymbol{\Psi}}$ is pertaining to viscous stress, and $D_Y = D_{Y_1} + D_{Y_2}$ is relevant to additional effects of mixture inhomogeneities.

Integrating Eq.(8) over the computational domain depicted in Fig. 1 leads to:

$$\frac{\partial \mathcal{E}_d}{\partial t} = \mathcal{W}_{in} - \mathcal{W}_{out} + \mathcal{D} \tag{9}$$

where the quantities $\mathcal{E}_d = \int_{\mathcal{V}} E_d \, dv$ and $\mathcal{D} = \int_{\mathcal{V}} D \, dv$ denote the disturbance energy and source term in the whole computational domain, while $\mathcal{W}_{in} = -\int_{\mathcal{S}(x=0)} \boldsymbol{W} \cdot d\boldsymbol{S}$ and $\mathcal{W}_{out} = \int_{\mathcal{S}(x=L)} \boldsymbol{W} \cdot d\boldsymbol{S}$ stand for the corresponding inlet and outlet fluxes, respectively.

At this level, it is noteworthy that 320 datasets were extracted over 80 ms from the numerical simulation[3]. The post-processing first consists in extracting the variables fluctuations $(\,)_1$ by substracting the corresponding baseline values $(\,)_0$. Subsequently, the various terms of Eq.(8), which are detailed in the first and second columns of Tab. 3, are computed at each location and time step. Volume integration then yields the various contributions that appear in Eq.(9). Finally, the third column of Tab. 3 reports their time-averaged values, normalized by the time-averaged value of the disturbance energy, i.e., $\alpha_j = \overline{\mathcal{D}}_j / \overline{\mathcal{E}}_d$, thus quantifying their respective weigths in the total disturbance energy variation.

It is noteworthy that three contributions display significant growth-rate values: (i) D_{s1} and (ii) D_Q^{comb}, which are positive and associated to entropy and direct combustion source terms, and (iii) D_Q^{cond} which is negative and relevant to molecular damping effects induced by thermal diffusivity. It is noteworthy that these three leading-order contributions do involve temperature (entropy) fluctuations.

The possible influence of computational (i.e., spatial and temporal) resolution has been evaluated by varying the computational mesh size and time step. The impact of these variations is evaluated by considering the thermoacoustic source

[3]This corresponds to 8 imposed oscillation periods, with 40 points per period.

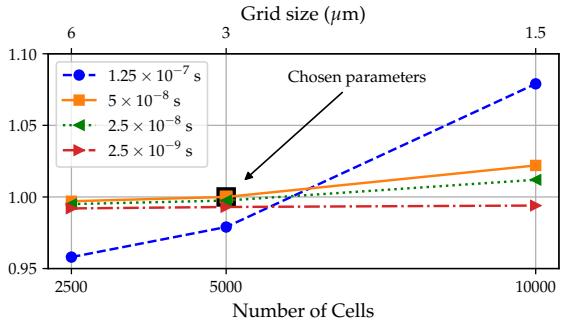

Figure 3: Thermoacoustic source normalized with respect to its reference value $\overline{\mathcal{D}}_Q^{comb}/\mathcal{D}_{Q,ref}^{comb}$ plotted as a function of the mesh refinement for several time steps

term which is one of the leading-order terms in the DEB (see Tab. 3). Three distinct computational grids and four time step values have been investigated. The values of Δx has thus been varied between 1.5 μm (10 000 grid points) and 6 μm (2 500 grid points), and the time step Δt between 2.5 ns and 125 ns. Figure 3 displays the thermoacoustic source term value $\overline{\mathcal{D}}_Q^{comb}$ normalized with respect to its value obtained in the reference simulation, which is $\mathcal{D}_{Q,ref}^{comb} = 4506$ W. Provided that the time step value remains sufficiently small (i.e., $\Delta t < 5 \cdot 10^{-8}$ s), it is found that the corresponding normalized source term is no longer dependent on the spatial resolution Δx. Thus, the retained computational mesh size and time step $(\Delta x, \Delta t) = (3\ \mu\text{m}, 5 \cdot 10^{-8}\ \text{s})$ appear as the best compromise between numerical accuracy and computational costs. With these values, a large number of numerical simulations – approximatively two hundreds – have been performed to conduct the parametric study reported in forthcoming sections 4 and 5.

4. Effect of flame motion

In this section, the sensitivity of the DEB to the inlet forcing given by Eq.(7) is investigated. Five distinct forcing frequencies $f \in [50; 100; 200; 400; 800]$ Hz are

considered while the value of η is increased by a factor $\Delta\eta = 0.05$ within the range $[0.01, 2.01]$. It is noteworthy that the possible range of variation of these parameters is restricted by the computational domain size and resolution: the upper boundary of the flame flapping width is indeed determined by the length of the computational domain whereas the computational resolution (i.e., the mesh cell size) imposes its lower boundary. It is also worth noting that, for the largest values of η, the inlet flow velocity is reversed. In this respect, it can be readily shown that the root-mean square (RMS) of the imposed inlet velocity variation u_{RMS} is equal to $\sqrt{\pi}\,\eta\,S_L^0$, which leads to $u_{\mathrm{RMS}} = 3.5\,S_L^0$ for the largest value $\eta = 2.01$. Such a value of u_{RMS} is not irrelevant to actual combustion devices. Flow velocities (and associated levels velocity fluctuations) in actual combustors may indeed be far greater than the laminar flame propagation velocity. In this respect, it is also noteworthy that inlet flow reversal may even be triggered by combustion instabilities as it occurs during flashback processes [43].

For the simulations post-processing, the dataset characteristics were kept the same as those retained in section 3, i.e., 320 datasets gathered over eight imposed oscillation periods. Subsection 4.1 first settles some definitions that are introduced to characterize the flame dynamics. Then, subsection 4.2 is devoted to the analysis of the DEB sensitivity according to this framework.

4.1. Flame dynamics modelling

Flame dynamics should first be properly characterized. Let us denote by χ any relevant variable (e.g., the heat release rate) and by χ_0 its reference value in the absence of any inlet forcing (steady-state value). Figure 4 provides, at a given time t^*, a qualitative picture of the spatial distribution of χ (when the flow is forced) together with its steady-state spatial distribution χ_0. The superscript $*$ corresponds to non-dimensional quantities. Thus, the coordinate x, flame thickness δ_L, and flame

position x_F have been made non-dimensional using the steady one-dimensional laminar premixed flame thickness of reference δ_L^0, and the time is normalized with the forcing pulsation in such a manner that $t^* = 2\pi f t$.

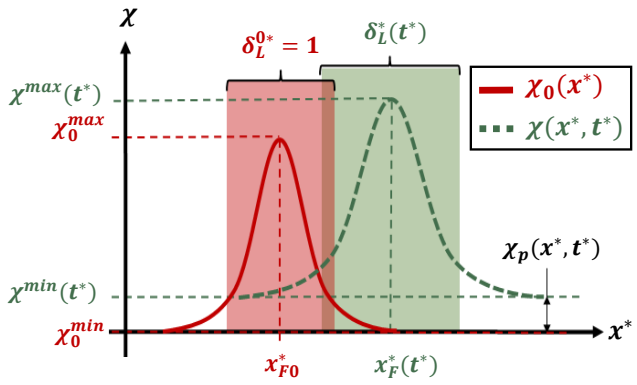

Figure 4: Spatial distribution of a generic variable χ in the reference case (red) and a pulsed case (green)

Following the picture of Fig. 4, flame dynamics is modelled on the basis of a given set of geometric transformations:

- ***Flame motion (FM)*** which is associated to the displacement or shifting of the flame location $\Delta x_F^* = x_{F,0}^* - x_F^*(t^*)$:

$$\chi^{FM}(x^*, t^*) = \chi_0\left(x^* - \Delta x_F^*(t^*)\right) \tag{10}$$

- ***Flame intensity response (FIR)***, without any consideration of flame wrinkling, which evaluates the gain $G_\chi(t^*)$ for the corresponding quantity χ

$$\chi^{FIR}(x^*, t^*) = G_\chi(t^*)\chi_0(x^*) \tag{11}$$

- ***Flame thickening (FT)*** which is relevant to the temporal variation of the

flame thickness:

$$\chi^{FT}(x^*,t^*) = \chi_0\left(\delta_L^*(t^*)x^*\right) \tag{12}$$

- ***Additional perturbations (AP)***, an offset induced by an external forcing, excluding the flame dynamics:

$$\chi^{AP}(x^*,t^*) = \chi_0(x^*,t^*) + \chi_p(x^*,t^*) \tag{13}$$

Finally, based on the consideration of all these effects, one may propose the following expression:

$$\chi(x^*,t^*) = G_\chi(t^*)\chi_0\left(\delta_L^*(t^*)\left[x^* - \Delta x_F^*(t^*)\right]\right) + \chi_p(x^*,t^*) \tag{14}$$

It should be emphasized that this expression (i.e., Eq.(14)) is as approximate as the picture given by Fig. 4 but it is however quite useful for the purpose of the present study.

Figure 5 displays four instantaneous profiles for the case f = 100 Hz and η = 0.21. The temporal evolution of combustion-induced HRR, see Fig. 5(a), is dictated solely by the flame motion, with no additional perturbation and negligible contributions of flame thickening and FIR. This is in contrast to the imposed velocity perturbations, which are transported and clearly visible at the end of the computational domain, see Fig. 5(c). Finally, it is worth noting that the maximal level of temperature is not quantitatively altered by the imposed perturbation, see Fig. 5(b).

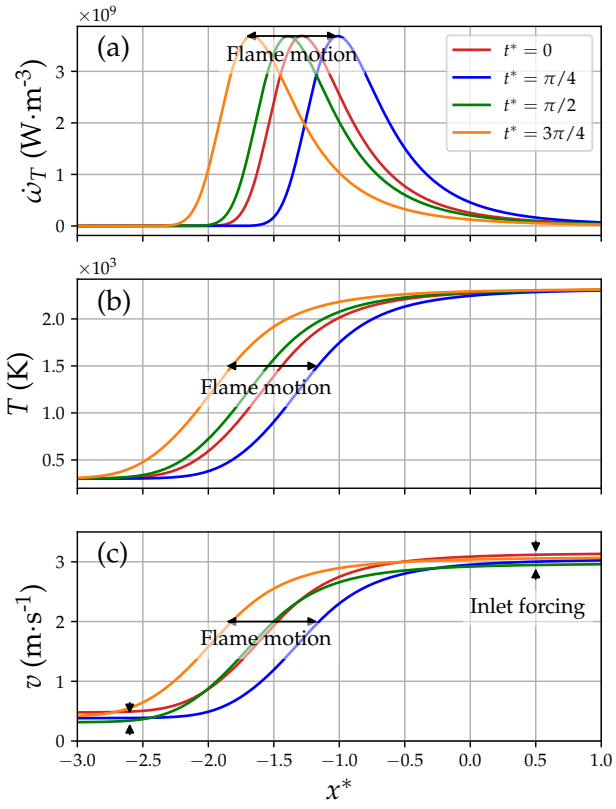

Figure 5: Temporal evolution in the case $(f,\eta) = (100\,\text{Hz}, 0.21)$. (a): combustion-induced HRR. (b): temperature. (c): velocity

4.2. Impact on the disturbance energy budget (DEB)

290 The formalism introduced above is now used to analyze the sensitivity of the DEB source terms to the inlet forcing parameters f and η. First, the assumptions made to describe the flame dynamics, see Fig. 5, are further investigated.

Flame motion being *a priori* relevant to any variable fluctuations, it can be assumed that (i) it is directly related to the inlet velocity periodic forcing and (ii) the flame displacement speed writes $v_F(t) = v(x=0,t) - S_L^0 = \eta S_L^0 \cos(2\pi f t)$. Thus,

its displacement Δx_F may be deduced from:

$$\Delta x_F(t) = \int_{t_0}^{t} v_F(t)dt = \int_{t_0}^{t} \eta S_L^0 \cos(2\pi f t)dt = \frac{\eta S_L^0}{2\pi f}\left[\sin(2\pi f t) - \sin(2\pi f t_0)\right] \quad (15)$$

If we consider an initial time t_0 that corresponds to an entire number of imposed oscillation periods, the flame displacement is given by the following non-dimensional expression:

$$\Delta x_F^*(t^*) = \frac{\sin(t^*)}{\mathrm{St}} \quad (16)$$

where

$$\mathrm{St} = \frac{2\pi f \delta_L^0}{\eta S_L^0} \quad (17)$$

is a Strouhal number based on the flame thickness δ_L^0, the pulsation of the fluctuation $2\pi f$, and the amplitude of the acoustic forcing ηS_L^0. As it is defined, this dimensionless number decreases as the amplitude of flame motion increases. As a consequence, its smallest values are dictated by the length of the computational domain whereas its largest values are restricted by the resolution of the computational mesh. As it is defined, the Strouhal number St is proportional to f/η, so reaching higher values of St would mean either increasing the frequency of the perturbation or decreasing its amplitude. Some studies devoted to the high-frequency response of flames – see for instance reference [37] – have previously explored conditions relevant to larger values of St. In this respect, it is also noteworthy that another Strouhal number $St_F = f\delta_L^0/S_L^0$ may be used to characterize the local quasi-steadiness of the flame [37]. In our simulations, its values reaches approximately 0.90 for the 800 Hz frequency. In this respect, it is noteworthy that, for high-frequency conditions – which correspond to values of St_F larger than unity – the burning velocity (and FIR) could be altered in the general (and multi-dimensional)

case. This is however outside the scope of the present study, which is focused on the flame motion (FM) effects as triggered by inlet velocity fluctuations.

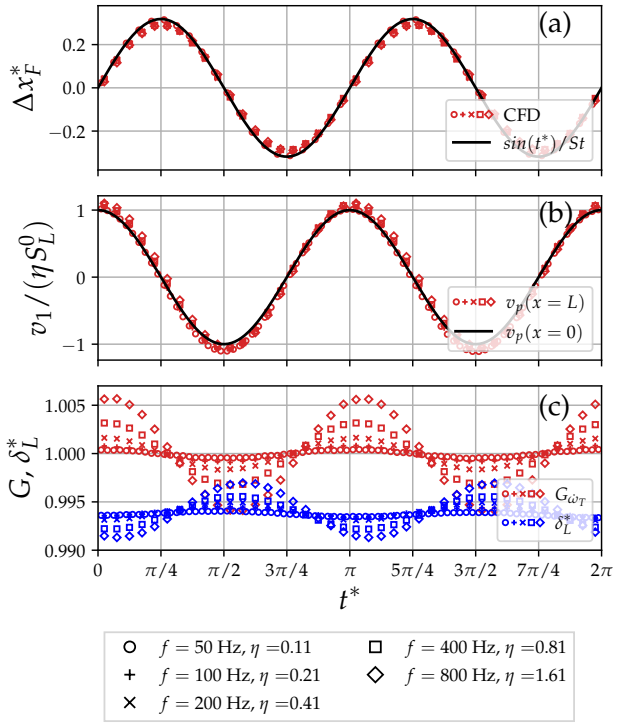

Figure 6: Temporal variation of the flame dynamics characteristics in various cases relevant to St = 3.04 ± 0.14. Comparisons between CFD data (symbols) and models (lines). (a): flame motion, (b): velocity perturbation normalized by the forcing amplitude ηS_L^0, and (c): flame intensity response (FIR) together with flame thickening

Figure 6 displays the temporal evolution of the quantities introduced in Eqs.(10)-(13). For each value of the forcing frequency, the value of the amplitude η has been chosen so as to keep the value of the Strouhal number St approximately constant and close to 3.04. As it can be seen in Fig. 6(a), whatever the value of the frequency, the variations of Δx_F^* follow closely the relation given in Eq.(16), thus confirming that flame motion is dictated by the imposed inlet velocity oscillations. As shown in Fig. 6(b), additional perturbations do also appear to be mostly determined by the

imposed oscillations, e.g., the values observed at the computational domain outlet remain close to those imposed at its inlet, i.e., $v_p(0,t) = \eta S_L^0 \cos(2\pi f t)$. Figure 6(c) reports the evolutions of the flame thickness and HRR gain. With only one percent maximal shift, flame thickening effects and FIR can be considered as negligible: only flame motion and transported velocity perturbations $v_p(x,t)$ need to be taken account.

Finally, from the above analysis, the different variables can be split into two distint categories: (i) those for which only FM needs to be considered, e.g., the HRR, as displayed in Fig. 5(a), and (ii) those for which AP is relevant through transported velocity perturbations (hereafter referred to as VP), see Fig. 5(c). Thus, the DEB source terms are split into either (i) flame dynamics (FD) terms, which are related only to variations of the flame location, or (ii) velocity perturbation (VP) terms.

4.2.1. Flame dynamics related terms

Since the flame structure is found unaltered by the imposed perturbation, see Figs. 5 and 6, flame dynamics (FD) is governed by flame motion (FM). Thus, the temporal variation of any variable χ driven by flame dynamics (FD) – or, put in other words, flame motion (FM) – can be written as follows:

$$\chi(x^*,t^*) = \chi_0\left(x^* - \frac{\sin(t^*)}{\mathrm{St}}\right) \tag{18}$$

with $\chi_1(x^*,t^*) = \chi(x^*,t^*) - \chi_0(x^*)$ the associated fluctuation. If two variables driven by the flame motion are considered, their cross-correlations, as well as the source terms involving these two quantities, should only depend on x^*, t^*, and St. Thus, one may anticipate that the flame-motion Strouhal number (introduced above) drives the terms D_{s1}, D_Q, D_{Q^*}, D_{Y_2}, and W_2.

4.2.2. Velocity-forcing dependent terms

The VP terms represent the perturbation energy which is a direct outcome of the inlet forcing. For a given value of η, their growth-rate is negligible. However, it has been shown in the literature [16, 15] that some source terms associated to a negligible growth-rate may play a major role in the system dynamics by leading to a non-negligible time lag. Thus, to estimate possible time lag effects, a comparison between the maximum levels of various source terms is performed below.

Figure 7 displays the dimensionless ratios of the maximum values $|\mathcal{D}_{s_2}|_{max}$ and $|\mathcal{D}_Q^{comb}|_{max}$ normalized by the maximum of $\partial\mathcal{E}_d/\partial t$, plotted versus $1/\mathrm{St}$, which should render more adequately than growth-rates the VP terms instantaneous contributions. For the largest values of $1/\mathrm{St}$ (highest forcing amplitudes), the contribution $\mathcal{D}_{s_2}$, the growth-rate of which is negligible for the reference flame (see Tab. 3), becomes significant and thus cannot be neglected. It is concluded that $\mathcal{D}_{s_2}$ should be added to the sources having important growth-rates (previously described in section 3) in order to describe satisfactorily the flame response whatever the regime, and the following set of terms must therefore be retained: $\mathcal{D}_{s1}$, $\mathcal{D}_Q^{comb}$, $\mathcal{D}_Q^{cond}$, and $\mathcal{D}_{s_2}$.

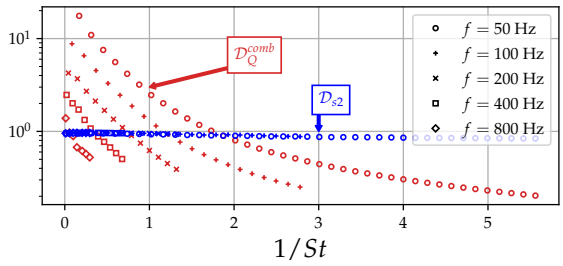

Figure 7: Orders of magnitude of $\mathcal{D}_Q^{comb}$ and $\mathcal{D}_{s_2}$ defined as $O(\mathcal{D}) = |\mathcal{D}|_{max}/(\partial\mathcal{E}_d/\partial t)_{max}$ plotted versus $1/\mathrm{St}$

The term $\mathcal{D}_{s_2}$, like other terms present in Tab. 3, is dependent upon the velocity forcing through a cross correlation $\chi_1 m_1$ associated to the mass flux fluctuations

$m_1 = (\rho v)_1$, with χ_1 being a FD variable. The specificity of this term is to depend explicitly on velocity fluctuations, and thereby on velocity perturbations $v_p(x^*, t^*)$ which should be added to the flame motion contribution $v_0\,(x^* - \sin(t^*)/\mathrm{St})$. Thus, the mass flux $m = \rho v$ writes:

$$m = \rho_0 v_0 \left(x^* - \frac{\sin(t^*)}{\mathrm{St}} \right) + \rho_0 \left(x^* - \frac{\sin(t^*)}{\mathrm{St}} \right) v_p(x^*, t^*) \tag{19}$$

From the one-dimensional mass conservation equation, it is readily shown that $m_0 = \rho_0 v_0$ is constant along x^*. Thus, the mass flux fluctuation $m_1 = m - m_0$ writes:

$$m_1 = \rho_0 \left(x^* - \frac{\sin(t^*)}{\mathrm{St}} \right) v_p(x^*, t^*) \tag{20}$$

As it can be seen in Fig. 6(b), the inlet velocity perturbation is shown to be recovered at the computational domain outlet. Therefore, v_p can be approximated from the following expression:

$$v_p(x^*, t^*) = v(x^* = 0, t^*) = \eta S_L^0 \cos(t^*) \tag{21}$$

Substituting Eq.(21) into Eq.(20) leads, after some algebra, to the following expression of the cross-correlation $\chi_1 m_1$:

$$\frac{\chi_1 m_1}{\eta} = S_L^0 \cos(t^*) \chi_1 \rho_0 \left(x^* - \frac{\sin(t^*)}{\mathrm{St}} \right) \tag{22}$$

with χ_1 a FD variable verifying Eq.(18). Thus, the VP terms (i.e. D_{s_2}, D_{Y_1}, and W_1) are functions of both St and η, in such a manner that D_{VP}/η is a function of St.

4.3. Classification of the sources

According to the above analysis, the temporal evolution of flow variables appears to be led by either flame dynamics (i.e., flame motion in the present case) or external perturbations (inlet velocity forcing). Sources of disturbance energy do involve cross-correlations between unsteady flow variables and, as a consequence, also fall into these two categories (FD and VP). Table 4 describes their classification on the basis of the DEB framework retained herein [16, 14].

Table 4: Classification of the DEB sources as either FD or VP terms. St is the invariance parameter for FD source terms. For VP terms, St is the invariance parameter for these terms once normalized by η

Flame dynamics (FD)	Velocity perturbation (VP)	Other
D_{s_1}, D_Q^{comb}, D_Q^{cond}, D_Q^{sp}, D_{Q^*}, D_{Y_2} $\boldsymbol{W_2}$	D_{s_2}, D_{Y_1}, $\boldsymbol{W_1}$	$D_{\boldsymbol{\Omega}}$, $D_{\boldsymbol{\Psi}}$

Invariance with respect to the flame motion Strouhal number St can be obtained for the terms gathered in the two first columns of Tab. 4. However, this does not hold for $D_{\boldsymbol{\Omega}}$ and D_Ψ because the dependence of $\boldsymbol{\nabla} \wedge \boldsymbol{\Omega}$ and $\boldsymbol{\tau}$ on the dimensionless numbers St and η is more complicated.

5. Parametric analysis

The conclusions drawn from the above analysis are now used as a basis for conducting a parametric study. The parametric study is focused on the evolution of $D_Q^{comb} = T_1 \, (\dot{q}/T)_1$ and $D_{s_2} = -\nabla T_0 \, m_1 \, s_1$ as relevant of the FD and VP source terms gathered in Tab. 4. The inlet velocity forcing being periodic, Fourier analysis has been applied to these source terms and their harmonics will be considered together with their time-averaged values in the following analysis.

5.1. Global properties

Figure 8 displays, for the whole set of computational data, the evolution of some volume-integrated quantities plotted versus $1/\mathrm{St}$. In Fig. 8(a), the fluctuating energy $\overline{\mathcal{E}}_d$ and its harmonics are found to increase with $1/\mathrm{St}$. Provided that St is kept constant, the various plots are all superimposed whatever the values of the frequency f and amplitude η. At this level, it is noteworthy that the first harmonic ($1f$) represents the energy contained in the difference between the time-average flow and the baseline flow (the time-averaged fluctuations $\overline{(\,)}_1$ do not cancel). The second harmonic $2f$ is relevant to the linear contribution of the system to disturbance energy. Since the inlet perturbation is a single-frequency signal, higher-order harmonics ($3f$, $4f$, ...) are the direct consequence of the non-linear nature of heat-release dynamics.

For large amplitude flame motion, the linear contributions (second harmonics) are transferred into non-linear ones. The number of significant higher-order harmonics ($4f$, $6f$...) thus increases with $1/\mathrm{St}$. The growth-rate is a decreasing function of $1/\mathrm{St}$, see Fig. 8(b). For the FD terms odd harmonics ($1f$, $3f$, ...), the similarity based on the single dimensionless number St not strictly verified, see Fig. 8(c). However, if one excepts the smallest values of $1/\mathrm{St}$ (moderate flame motion) their amplitudes remain quite small compared to their even counterparts ($2f$, $4f$, ...). As it was expected from the previous section, the VP terms, once normalized by η, are mostly driven by St, see Fig. 8(d). These plots are indeed superimposed whatever the forcing frequency and amplitude.

5.2. Local properties

Figure 9 displays the spatial distribution of the thermoacoustic source term and η-normalized entropy source term together with their harmonics. Figures 9(a)-(e) thus report the corresponding quantities for almost constant values of St. Indeed,

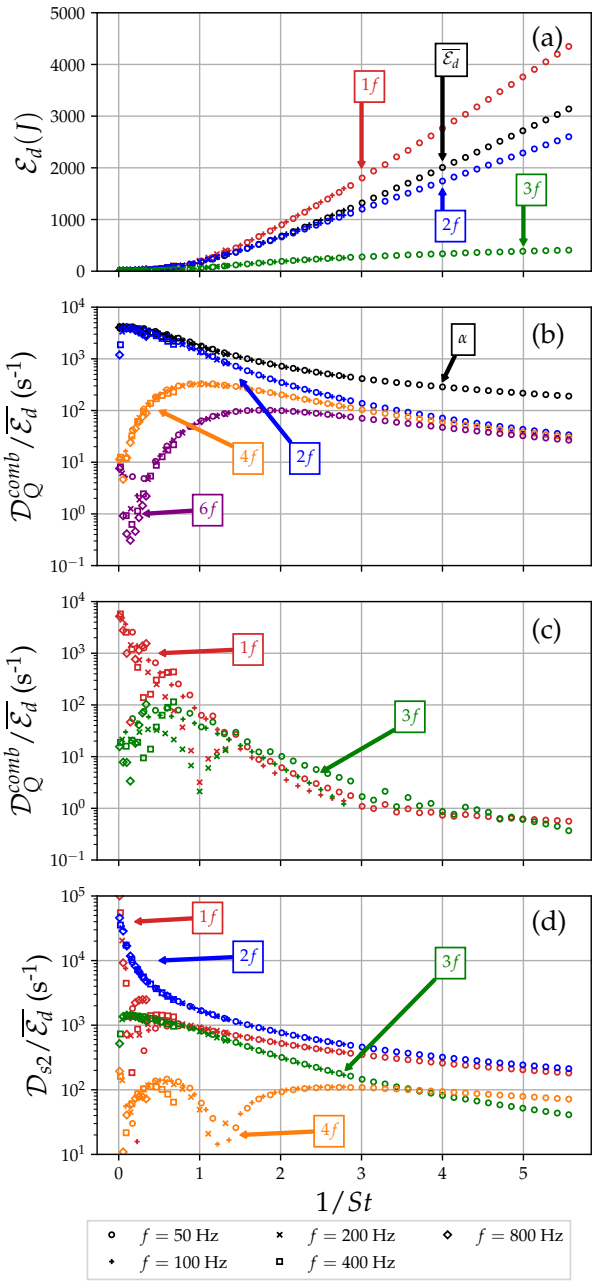

Figure 8: Dependence of the DEB source terms $\mathcal{D}_Q^{comb}$ and $\mathcal{D}_{s_2}$ on 1/St. Averaged quantities (black marks) and harmonics (colored marks, $1f$, $2f$, $3f$, $4f$, $6f$ frequencies). (a) Disturbance energy, (b) $\mathcal{D}_Q^{comb}$ growth-rate and its even harmonics, (c) $\mathcal{D}_Q^{comb}$ odd harmonics, (d) η-normalized $\mathcal{D}_{s_2}$ harmonics

for each plot, the values of f and η have been chosen to keep the value of St approximately constant. The abscissa-axis corresponds to the time-averaged progress variable $\overline{c}$, which is bounded between $\overline{c} = 0$ in the fresh reactants and $\overline{c} = 1$ in the burnt products.

This figure shows that the similarity features introduced in section 4.2 are also recovered in the local trends. For the lowest values of the Strouhal number, where the flame motion is greater than its thermal thickness (St < 1), the results are well described by a single curve. If the value of St is increased, the similarity may remain valid but only for a reduced range of frequencies, e.g. $50 - 200$ Hz for the case St = 1.556 ± 0.033, see Fig. 9.(c).

Furthermore, studying those local plots leads to a better interpretation of the sources:

- Two distinct flow regions are seen for the thermoacoustic source: (i) when $\overline{c}$ tends to zero, combustion acts as a source of disturbance energy ($\overline{D}_Q^{comb}$ is strictly positive) and (ii) when $\overline{c}$ tends to unity, combustion acts as a damping contribution: $\overline{D}_Q^{comb}$ is strictly negative. The harmonics also admit several nodes, corresponding to their phase inversion. If one excepts the $1f$ nodes which lie outside the frequency range of validity, all the nodes of $\overline{D}_Q^{comb}$ and its harmonics are St-invariants. The above-mentioned nodes, which correspond to the boundaries where the spectral contribution of unsteady combustion acts either as a source or as a damping contribution, exhibit thereby stronger invariance than the one observed for D_Q^{comb}.

- The term $D_{s_2} = -\nabla T_0 m_1 s_1$ results from the coupling between the imposed mass flow rate oscillations (m_1) and entropy oscillations (s_1), and it is relevant to regions featuring significant variations of the baseline temperature. It is clear that it does not exhibit the same behavior as D_Q^{comb}, as it is purely

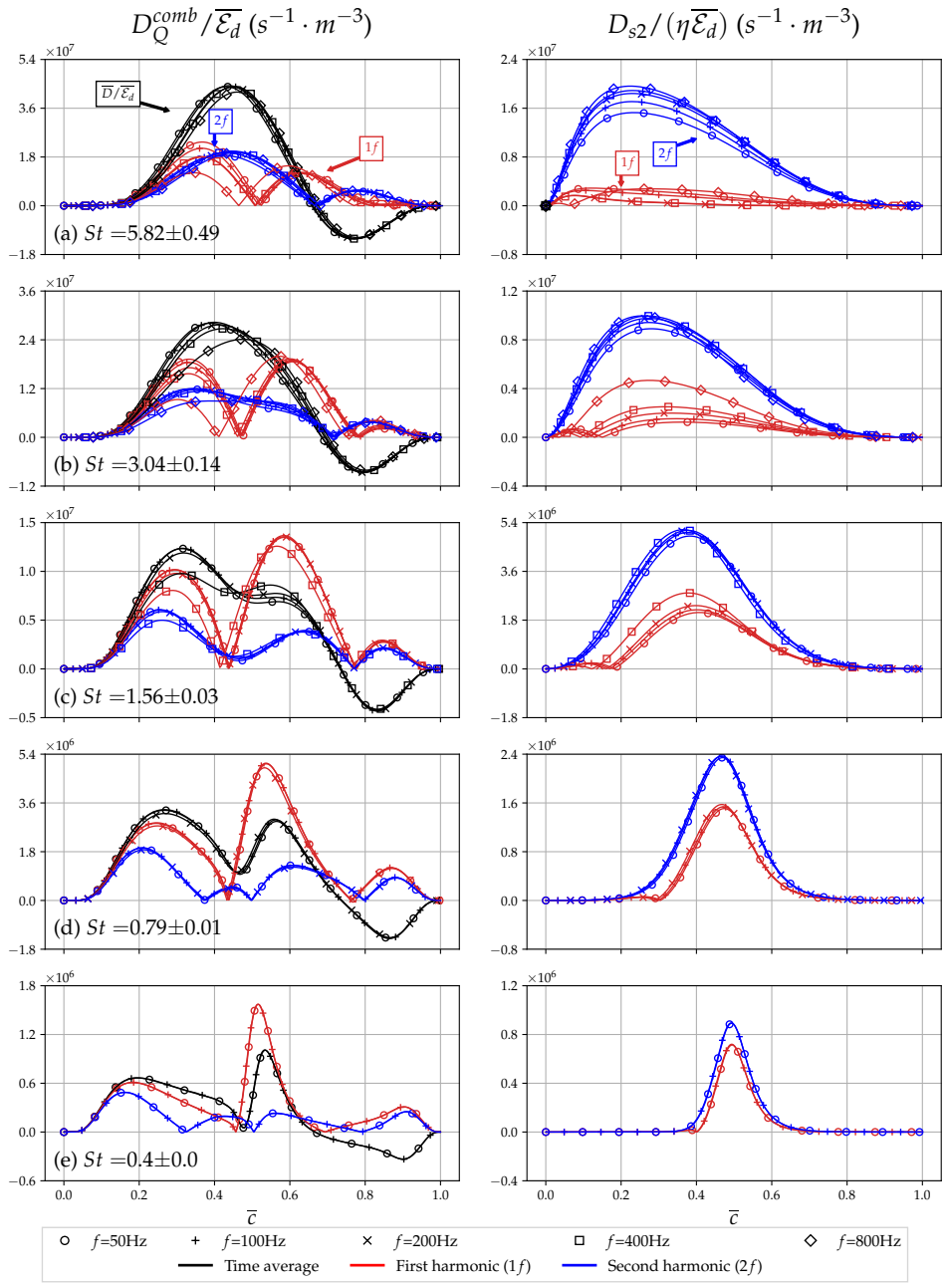

Figure 9: Profiles of $\overline{D}_Q^{comb}/\overline{\mathcal{E}}_d$ and associated harmonics (left) and $\overline{D}_{s_2}/(\eta\overline{\mathcal{E}}_d)$ and associated harmonics (right) for several values of St: (a) St = 5.823 ± 0.493, (b) St = 3.042 ± 0.135, (c) St = 1.556 ± 0.033, (d) St = 0.787 ± 0.007, and (e) St = 0.396 ± 0.001

transient (i.e., $\overline{D}_{s_2} = 0$) and not governed by the same set of invariance parameters (see Tab. 4). Its first harmonic ($1f$), which is smaller than its linear contribution ($2f$) for St = 5.823 ± 0.493 (see Fig. 9(a)) tends to become the same order of magnitude as the latter for decreasing values of St (see Figs. 9(b)-(e)). Moreover, by considering simultaneously the variations of $\overline{c}$ in the computational domain, it is found that, as St is decreased, the coupling term covers a less and less important part of the flame flapping zone and it is more and more constricted to a small region, which lies in the vicinity of $\overline{c} = 0.5$. This is in contrast to D_Q^{comb}, which is found to spread over the whole range of $\overline{c}$-variation.

5.3. Summary of the main results

The possible self-similarity characteristics that were introduced in section 4 have been scrutinized on the basis of numerical simulations results. Two disturbance energy source terms typical of flame dynamics (FD) and velocity perturbations (VP) have been analyzed. Some self-similarity trends were highlighted for both global and local quantities. Invariance is well assessed for cases featuring the lowest values of the Strouhal number St where flame motion is the most significant contribution. If the Strouhal number St is smaller than unity (i.e., flame flapping amplitude greater than its thermal thickness), the source terms distribution is found to be invariant. As a consequence, the source terms of the DEB can be deduced from any other computation performed for the same values of the two dimensionless numbers St and η, the dimensionless amplitude of the velocity fluctuations as given by Eq.(7).

6. Concluding remarks

Combustion instabilities are usually driven by flame dynamics, which can itself be associated to various contributions including flame motion, flame intensity response, etc. In this study, the focus is placed on the contribution of the flame motion, as triggered by a pulsed inlet velocity. The resulting flame motion leads to entropy variations. Thus, the disturbance energy budget (DEB) – taking into account entropy and mixture inhomogeneities perturbations – has been used to scrutinize the response to the inlet velocity forcing, the amplitude and frequency of which have been varied.

The following set of conclusions can be drawn from this analysis:

1. The response can be decomposed into two kinds of sources: (i) flame dynamics sources, with disturbances produced by the flame and its motion, and (ii) velocity perturbation terms, related to the disturbance energy produced by external velocity fluctuations.
2. These source terms are found to be mostly dependent on two dimensionless numbers that characterize (i) the laminar premixed flame motion (Strouhal number St) and (ii) the acoustic forcing η.
3. The flame dynamics is found to be predominant for sufficiently large values of the Strouhal number St but the terms driven by the velocity perturbation are no longer negligible for smaller values of St.
4. These conclusions are found to apply not only to time-averaged and volume-integrated quantities but also to their spatial distributions (including harmonics relevant to non-linearities) in the flame-flapping zone. Provided that the value of St remains sufficiently small (typically St < 1), the whole flame dynamics can thus be reconstructed from the knowledge of both non-dimensional numbers values (St and η) together with a reference flame ob-

tained for the same St and η.

However, the two dimensionless numbers mentioned above may not be sufficient to describe the non-linear behavior of the flame response from a general point of view. Indeed, it would be interesting to scrutinize this response in other conditions featuring either equivalence ratio or fresh reactants temperature fluctuations or in multi-dimensional reactive flows. Since the Strouhal number also depends on some characteristics of the flame, the effect of more realistic chemical kinetics and transport may also deserve further attention. It is also worth emphasizing that the acoustic forcing amplitudes that were studied herein remain rather moderate. Thus, the validity of this analysis now deserves to be assessed in other conditions featuring larger amplitudes (i.e., smaller Strouhal numbers).

Acknowledgments

The quality of the manuscript has benefited from the comments made by the reviewers. The authors gratefully aknowledge A. K. Mohamed, O. Dessornes, J. Anthoine, P. Villedieu, L. Jacquin from ONERA, and T. Coué from DGA for their support, as well as ONERA and AID (Contract DGA 2020 65 0022) for financial support.

References

[1] T. C. Lieuwen, Unsteady Combustor Physics, Cambridge University Press, 2012.

[2] A. A. Putnam, W. R. Dennis, A study of burner oscillations of the organ-pipe type, Trans. ASME 75 (1953) 15–26.

[3] A. A. Putnam, Combustion-Driven Oscillation in Industry, Elsevier, 1971.

[4] J. W. S. Rayleigh, The explanation of certain acoustical phenomena, Roy. Inst. Proc. 8 (1878).

[5] P. Clavin, G. Searby, Combustion Waves and Fronts in Flows, Cambridge University Press, 2016.

[6] T. Schuller, T. Poinsot, S. Candel, Dynamics and control of premixed combustion systems based on flame transfer and describing functions, J. Fluid Mech. 894 (2020) P1.

[7] S. W. Rienstra, A. Hirschberg, An Introduction to Acoustics, Eindhoven University of Technology, 2004.

[8] F. Nicoud, T. Poinsot, Thermoacoustic instabilities: Should the Rayleigh criterion be extended to include entropy changes?, Combust. Flame 142 (2005) 153–159.

[9] S. M. Candel, Acoustic conservation principles and an application to plane and modal propagation in nozzles and diffuser, J. Sound Vib. 41 (1975) 207–232.

[10] C. L. Morfey, Acoustic energy in non-uniform flows, J. Sound Vib. 14 (1971) 159–170.

[11] G. J. Bloxsidge, A. P. Dowling, N. Hooper, P. J. Langhorne, Active control of reheat buzz, AIAA J. 26 (1988) 783–790.

[12] B. T. Zinn, Pulse combustion: recent applications and research issues, Symp. (Int.) Combust. 24 (1992) 1297–1305.

[13] B. T. Chu, On the energy transfer to small disturbances in fluid flow (Part I), Acta Mech. 1 (1965) 215–234.

[14] M. K. Myers, Transport of energy by disturbances in arbitrary steady flows, J. Fluid Mech. 226 (1991) 383–400.

[15] A. Giauque, T. Poinsot, M. Brear, F. Nicoud, Budget of disturbance energy in gaseous reacting flows, in: Proceedings of the Summer Program, Center for Turbulence Research, NASA Ames/Stanford University, 2006, pp. 285–297.

[16] A. Giauque, Fonctions de transfert de flamme et énergies des pertubations dans les écoulements réactifs, Ph.D. thesis, Toulouse, INPT (2007).

[17] N. Karimi, M. J. Brear, W. H. Moase, Acoustic and disturbance energy analysis of a flow with heat communication, J. Fluid Mech. 597 (2008) 67–89.

[18] M. J. Brear, F. Nicoud, M. Talei, A. Giauque, E. R. Hawkes, Disturbance energy transport and sound production in gaseous combustion, J. Fluid Mech. 707 (2012) 53–73.

[19] L. S. Chen, S. Bomberg, W. Polifke, Propagation and generation of acoustic and entropy waves across a moving flame front, Combust. Flame 166 (2016) 170–180.

[20] Y. Song, J. Li, L. Yang, Effect of flame motion on longitudinal combustion instabilities, Aerosp. Sci. Tech. 122 (2022) 107427.

[21] K. J. George, R. I. Sujith, On Chu's disturbance energy, J. Sound Vib. 330 (2011) 5280–5291.

[22] K. J. George, R. I. Sujith, Disturbance energy norms: A critical analysis, J. Sound Vib. 331 (2012) 1552–1566.

[23] F. E. Marble, S. M. Candel, Acoustic disturbance from gas non-uniformities convected through a nozzle, J. Sound Vib. 55 (1977) 225–243.

[24] W. Polifke, C. O. Paschereit, K. Döbbeling, Constructive and destructive interference of acoustic and entropy waves in a premixed combustor with a chocked exit, Int. J. Acoust. Vib. 6 (2001) 135–146.

[25] Y. Méry, Impact of heat release global fluctuations and flame motion on transverse acoustic wave stability, Proc. Combust. Inst. 36 (2017) 3889–3898.

[26] Y. Méry, Dynamical response of a perfectly premixed flame and limit behavior for high power density systems, Combust. Flame 192 (2018) 410–425.

[27] L. Crocco, S. I. Cheng, Theory of combustion instability in liquid propellant rocket motors, Butterworths Scientific Publications, 1956.

[28] S. Candel, T. Poinsot, Flame stretch and the balance equation for the flame area, Combust. Sci. Technol. 70 (1990) 1–15.

[29] N. Peters, A spectral closure for premixed turbulent combustion in the flamelet regime, J. Fluid Mech. 242 (1992) 611–629.

[30] D. H. Shin, T. Lieuwen, Flame wrinkle destruction processes in harmonically forced, laminar premixed flames, Combust. Flame 159 (2012) 3312–3322.

[31] T. Schuller, D. Durox, S. Candel, A unified model for the prediction of laminar flame transfer functions: comparisons between conical and V-flame dynamics, Combust. Flame 134 (1-2) (2003) 21–34.

[32] D. Durox, T. Schuller, N. Noiray, S. Candel, Experimental analysis of nonlinear flame transfer functions for different flame geometries, Proc. Combust. Inst. 32 (2009) 1391–1398.

[33] T. Lieuwen, B. T. Zinn, The role of equivalence ratio oscillations in driving combustion instabilities in low NOx gas turbines, Symp. (Int.) Combust. 27 (1998) 1809–1816.

[34] J. G. Lee, K. Kim, D. A. Santavicca, Measurement of equivalence ratio fluctuation and its effect on heat release during unstable combustion, Proc. Combust. Inst. 28 (2000) 415–421.

[35] T. Sattelmayer, Influence of the combustor aerodynamics on combustion instabilities from equivalence ratio fluctuations, J. Eng. Gas Turbines Power 125 (2003) 11–19.

[36] T. Lieuwen, Modeling premixed combustion-acoustic wave interactions: A review, J. Propul. Power 19 (2003) 765–781.

[37] S. Shreekrishna, T. Lieuwen, High frequency premixed flame response to acoustic perturbations (AIAA Paper 2009-3261), in: 15th AIAA/CEAS Aeroacoustics Conference (30th AIAA Aeroacoustics Conference), 2009.

[38] F. Gant, A. Gruber, M. R. Bothien, Development and validation study of a 1D analytical model for the response of reheat flames to entropy waves, Combust. Flame 222 (2020) 305–316.

[39] A. C. McIntosh, Pressure disturbances of different length scales interacting with conventional flames, Combus. Sci. Technol. 75 (1991) 287–309.

[40] G. Ledder, A. K. Kapila, The response of premixed flames to pressure perturbations, Combust. Sci. Technol. 76 (1991) 21–44.

[41] J. Schwing, F. Grimm, T. Sattelmayer, A model for the thermo-acoustic feedback of transverse acoustic modes and periodic oscillations in flame position in cylindrical flame tubes (ASME Paper GT2012-68775), in: ASME Turbo Expo 2012: Turbine Technical Conference and Exposition, 2012.

[42] A. Genot, S. Gallier, T. Schuller, Thermo-acoustic instabilities driven by fuel droplet lifetime oscillations, Proc. Combust. Inst. 37 (2019) 5359–5366.

[43] J. O. Keller, L. Vaneveld, D. Korschelt, G. L. Hubbard, A. F. Ghoniem, J. W. Daily, A. K. Oppenheim, Mechanism of instabilities in turbulent combustion leading to flashback, AIAA J. 20 (1982) 254–262.

[44] H. M. Altay, R. L. Speth, D. E. Hudgins, A. F. Ghoniem, Flame–vortex interaction driven combustion dynamics in a backward-facing step combustor, Combust. Flame 156 (2009) 1111–1125.

[45] J. M. Klein, A. Genot, A. Vincent-Randonnier, A. Mura, Combustion thermoacoustics: on the relevance of some stability criteria (EUCASS Paper 2022-4361), in: Proceedings of the 9^{th} European Conference for Aeronautics and Space Sciences (EUCASS), Lille (France), 2022.

[46] S. Shreekrishna, S. Hemchandra, T. Lieuwen, Premixed flame response to equivalence ratio perturbations, Combust. Theory Model. 14 (2010) 681–714.

[47] J. H. Cho, T. Lieuwen, Laminar premixed flame response to equivalence ratio oscillations, Combust. Flame 140 (2005) 116–129.

[48] S. Shreekrishna, T. Lieuwen, Flame response to equivalence ratio fluctuations - relationship between chemiluminescence and heat release (AIAA Paper 2009-5058), in: 45th AIAA/ASME/SAE/ASEE Joint Propulsion Conference & Exhibit, 2009.

[49] H. Ax, W. Meier, Experimental investigation of the response of laminar premixed flames to equivalence ratio oscillations, Combust. Flame 167 (2016) 172–183.

[50] R. Lauvergne, F. N. Egolfopoulos, Unsteady response of C_3H_3/air laminar premixed flames submitted to mixture composition oscillations, Proc. Combust. Inst. 28 (2000) 1841–1850.

[51] A. L. Birbaud, S. Ducruix, D. Durox, S. Candel, The nonlinear response of inverted "V" flames to equivalence ratio nonuniformities, Combust. Flame 154 (2008) 356–367.

[52] T. Tomidokoro, T. Yokomori, H. G. Im, T. Ueda, Characteristics of counterflow premixed flames with low frequency composition fluctuations, Combust. Flame 212 (2020) 13–24.

[53] A. Refloch, B. Courbet, A. Murrone, P. Villedieu, C. Laurent, P. Gilbank, J. Troyes, L. Tessé, G. Chaineray, J. B. Dargaud, E. Quémerais, F. Vuillot, CEDRE software, AerospaceLab (2011) p1.

[54] G. Linassier, A. Bruyat, P. Villedieu, N. Bertier, C. Laurent, O. Rouzaud, R. Lecourt, H. Verdier, G. Lavergne, Application of numerical simulations to predict aircraft combustor ignition, CR Mecanique 341 (2013) 201–210.

[55] Y. Moule, V. Sabelnikov, A. Mura, M. Smart, Computational fluid dynamics investigation of a Mach 12 scramjet engine, J. Propul. Power 30 (2014) 461–473.

[56] Y. Moule, V. Sabelnikov, A. Mura, Highly resolved numerical simulation of combustion in supersonic hydrogen–air coflowing jets, Combust. Flame 161 (2014) 2647–2668.

[57] G. Pelletier, M. Ferrier, A. Vincent-Randonnier, V. Sabelnikov, A. Mura, Wall roughness effects on combustion development in confined supersonic flow, J. Propul. Power 37 (2021) 151–166.

[58] J. C. Butcher, Implicit Runge-Kutta processes, Math. Comp. 18 (1964) 50–64.

[59] C. Le Touze, A. Murrone, H. Guillard, Multislope MUSCL method for general unstructured meshes, J. Comp. Phys. 284 (2015) 389–418.

[60] C. S. Yoo, Y. Wang, A. Trouvé, H. G. Im, Characteristic boundary conditions for direct simulations of turbulent counterflow flames, Combust. Theory Model. 9 (2005) 617–646.

[61] N. Rutard, Simulation numérique et modélisation de l'influence d'ondes acoustiques de haute amplitude sur un jet diphasique: application au domaine de la propulsion fusée à ergols liquides, Ph.D. thesis, Paris-Saclay University (2019).

[62] C. K. Westbrook, F. L. Dryer, Simplified reaction mechanisms for the oxidation of hydrocarbon fuels in flames, Combust. Sci. Tech. 27 (1981) 31–43.

[63] A. Er-Raiy, Z. Bouali, J. Reveillon, A. Mura, Optimized single-step (OSS) chemistry models for the simulation of turbulent premixed flame propagation, Combust. Flame 192 (2018) 130–148.

[64] D. G. Goodwin, Cantera C++ user's guide, California Institute of Technology (2002).

[65] M. Huet, Budgets of disturbances energy for nozle flows ar subsonic and chocked regimes, J. Eng. Gas Turbines Power 140 (2018) 112602.